JOURNAL OF PROPULSION AND POWER
Vol. 23, No. 1, January–February 2007

Microwave Electrothermal Thruster Performance

Kevin D. Diamant,* Byron L. Zeigler,† and Ronald B. Cohen‡
The Aerospace Corporation, Los Angeles, California 90009

DOI: 10.2514/1.19571

Thrust, specific impulse, thrust efficiency, and coupling efficiency were measured for a nominally 1 kW microwave electrothermal thruster operating on He, N_2, and N_2O, and for a 5 kW model operating on water. For He, N_2, and N_2O, thrust varied from approximately 100 to 700 mN at discharge pressures from 6.7×10^4 to 2.7×10^5 Pa and magnetron input powers from 900 to 1500 W. Thrust measurements agree well with calculations assuming one-dimensional, isentropic flow of a perfect gas with constant specific heats. Peak specific impulses for He, N_2, and N_2O were 418, 243, and 209 s, respectively. Water was run at magnetron input powers from 2.1 to 4.1 kW and discharge pressures from 4.0×10^4 to 1.5×10^5 Pa. Thrust varied from approximately 100 to 250 mN with a peak specific impulse of 428 s. Incorporating an impedance matching capability improved coupling efficiency with water to over 96%, but did not increase specific impulse. Measurements with a residual gas analyzer indicate that the water plume may be 50 to 70% dissociated, and that the lack of dependence of specific impulse on specific energy results from a tradeoff between dissociation losses at low specific energy and heating of the thruster body at high specific energy.

I. Introduction

HIGH density, low toxicity, wide availability, and ease of storage and transport make water an attractive rocket propellant. High specific impulse and the ability to run water directly without first generating H_2 and O_2 are advantages that may be realized in an electric thruster. Given the low molecular weight and corrosive nature of water at high temperature, an electrodeless, electrothermal thruster may be best suited for this application.

The use of microwave sustained plasmas for propellant heating in electrothermal thrusters has been researched extensively over the past three decades [1–9]. Nitrogen, helium, hydrogen, and argon have been the most commonly studied propellants in the so-called microwave electrothermal thruster (MET); however, the rigidity of the components used to transfer microwave power to the applicator, as well as the desire to retain the capability to vary applicator geometry during operation, has precluded the use of conventional thrust stand measurements for performance evaluation. In this work, thrust stand measurements were possible through the use of a simplified thruster design, first suggested by Sullivan et al. [10], then implemented by Brandenburg and Micci [11], and through the use of a "momentum trap" mounted on a thrust stand. Thrust, specific impulse, thrust efficiency, and microwave coupling efficiency will be presented for a MET running on He, N_2, N_2O, and water. We will also discuss results obtained with a residual gas analyzer that allowed estimation of the level of dissociation in the MET water exhaust, yielding valuable insight into water MET power partitioning.

II. Experiment

A. Facility

The MET was installed in a 75 cm diam by 1.2 m long vacuum chamber pumped by two roots blowers in series backed by up to eight rotary piston pumps. Chamber pressure for all conditions reported varied from approximately 5 to 21 Pa. At these background pressures the MET nozzle was in all cases underexpanded.

Received 19 August 2005; revision received 23 February 2006; accepted for publication 26 February 2006.

*Senior Member of Technical Staff, Propulsion Science and Experimental Mechanics, M5-754. Member AIAA.

†Senior Research Associate, Propulsion Science and Experimental Mechanics, M5-754.

‡Director, Propulsion Science and Experimental Mechanics, M5-754. Member AIAA.

B. MET

The MET (Fig. 1) was based on a design published by Sullivan and Micci [12]. The cavity was sized to support the TM_{011} resonant mode, with an electric field maximum at each end of the cavity, on the cavity axis. The cavity was divided by a low loss boron nitride (BN) plate, allowing the section coupled to the microwave source to be maintained at atmospheric pressure, ensuring that gas breakdown would occur only at the maximum adjacent to the nozzle. Following breakdown, the plasma electrons absorbed the microwave power very efficiently and transferred it to atomic or molecular species by collisions. Propellant injected into the discharge chamber and heated in this manner was exhausted through a conical converging-diverging nozzle (Fig. 2). A graphite nozzle was used while running He, N_2, and N_2O. Water rapidly eroded the graphite nozzle, necessitating a switch to anodized aluminum. Throat diameters were 1.14, 1.32, and 1.57 mm for water, and 1.32 mm for the other propellants.

Microwave power at 2.45 GHz was supplied in two configurations. In the first, a magnetron was mated directly to the cavity. This compact configuration [10,11] had no impedance matching capability, yet still achieved efficient power absorption due to the resonance broadening effect of the high pressure plasma [1,2,4,13,14]. Two magnetrons were used in this configuration: a nominally 1 kW model obtained from a commercial microwave oven was used to test He, N_2, and N_2O, and a nominally 5 kW model was used to test water. To investigate the effect of improved microwave coupling efficiency on performance, a more conventional configuration incorporating an isolator and a 3-stub tuner was tested with the 5 kW magnetron. A section of waveguide welded into a flange carried microwave power into the vacuum chamber. At the thruster, the rectangular waveguide transitioned to the coaxial line, the center conductor of which was fitted with a hemispherically tipped sleeve that served as the coupling probe. Cavity geometry was fixed, and the stub tuner was relied upon exclusively for impedance matching.

C. Propellant Delivery

The propellant delivery system is diagrammed in Fig. 3. A thermal mass flow meter was used to measure He, N_2, and N_2O flow rates. The meter was calibrated in place by timing the rise of soap bubbles in a 1.5 liter graduated tube.

Steam was delivered to the MET by a steady flow system similar to Morren's design for the water vapor resistojet [15]. Distilled water was supplied from an N_2 pressurized 500 ml buret, and liquid flow rate was determined by measuring the pressure drop across a set of commercial flow restrictors. Flow calibration was performed by timing the accumulation of water in a 5 ml pipette. Water was

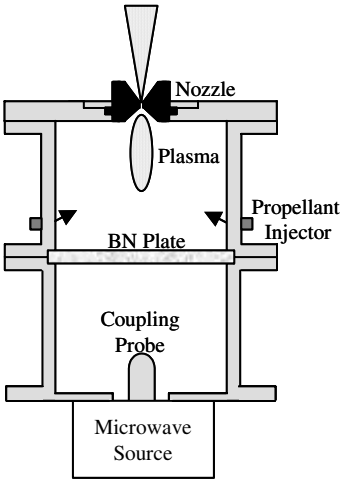

Fig. 1 MET diagram.

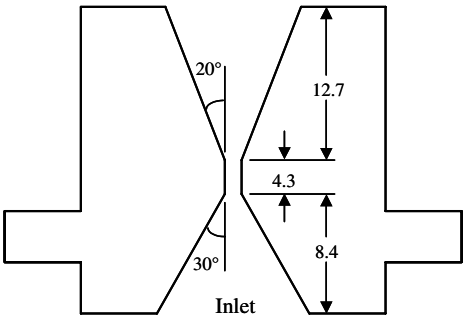

Fig. 2 MET nozzle cross section, dimensions in mm.

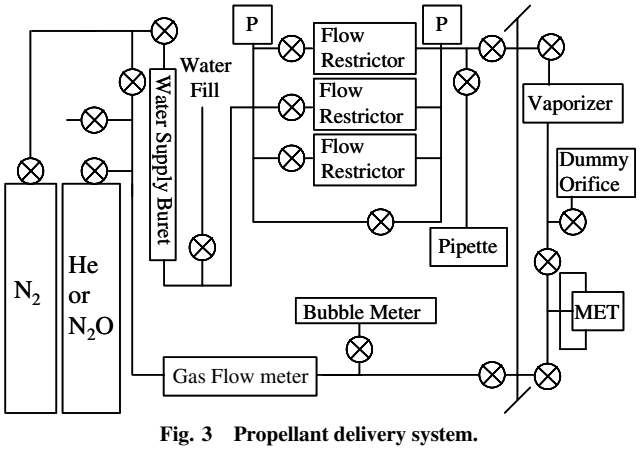

Fig. 3 Propellant delivery system.

converted to steam at the thruster by a packed bed vaporizer (Fig. 4) consisting of a cartridge heater enclosed in a stainless steel tube. Water entering the vaporizer was divided into four equally spaced inlets, then forced to flow over 0.35 mm diam glass beads packing the space between the heater and tube. Feed lines downstream of the vaporizer, as well as the plasma-containing section (discharge chamber) of the MET, were wrapped with heaters and maintained at greater than 100°C to prevent condensation. Feed line and discharge chamber heater power was reduced or eliminated as the thruster warmed up during operation.

Propellant was admitted to the MET through three equally spaced injection ports located near the base of the discharge chamber. Injection was tangential to the wall to generate a vortex flow for discharge stabilization [16]. All ports were in use for testing of He,

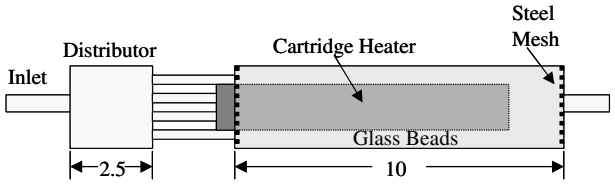

Fig. 4 Vaporizer, dimensions in cm.

N_2, and N_2O. Water was injected through just two of the ports, while the third was reserved for He during startup, as will be described in the next section. A capacitance manometer was attached directly to the discharge chamber to monitor pressure.

D. Thrust Measurements

For operation with the 1 kW magnetron, it was possible to mount the MET directly to the thrust stand, as diagrammed in Fig. 5. The stand was an inverted pendulum, configured as a hinged parallelogram. The top plate of the parallelogram rested on the thrust sensor, a strain gauge based load cell. A second load sensor was mounted beneath the thruster and was used to calibrate the stand by measuring loads applied by a stepper motor drawing up a line attached to it through a spring. Not shown in Fig. 5 are propellant and cooling water lines, which were fixed to the lower, stationary plate, then bent into a wide corkscrew before attaching to the upper plate. For each operating condition, thrust was measured at steady state, and then the thruster was turned off and the stand calibrated. Calibration consisted of checking the zero, applying three loads surrounding the measured value, and rechecking the zero.

The larger size of the 5 kW magnetron and, in the tunable configuration, the physical constraint of the rigid waveguide prevented direct use of the thrust stand. Instead, a momentum trap [17] was mounted on the stand, and the MET exhaust was directed into it from a distance of approximately 1.3 cm (Fig. 6). The trap was a steel can, 11.4 cm long by 7.6 cm in diameter, with a 2.5 cm diam entrance aperture. At the base of the can was a 45 deg cone. Two rows of 12 1.3 cm diam vent holes were located 1.3 and 3.2 cm behind the entrance plane. An attempt was made to validate this approach by comparing He and N_2 measurements with the trap to data recorded with the 1 kW MET mounted to the thrust stand (Fig. 7). Agreement between the two methods was obtained to within approximately 5%.

E. Residual Gas Analyzer

A crude attempt to determine the level of dissociation in the water plume was devised as follows. Two 3 mm diameter copper tubes were positioned to sample the effluent from two of the momentum

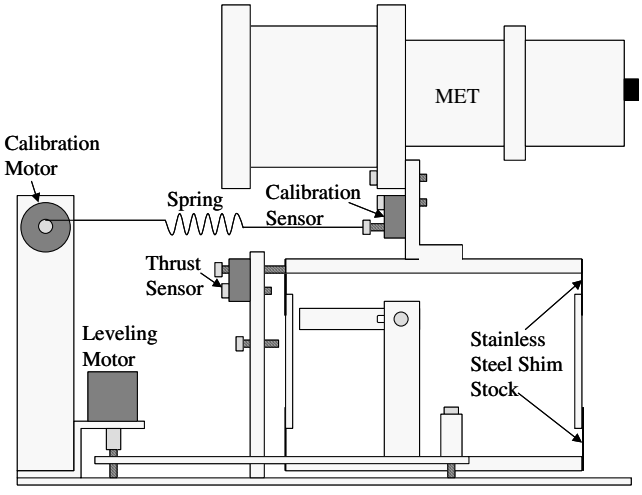

Fig. 5 1 kW MET on thrust stand.

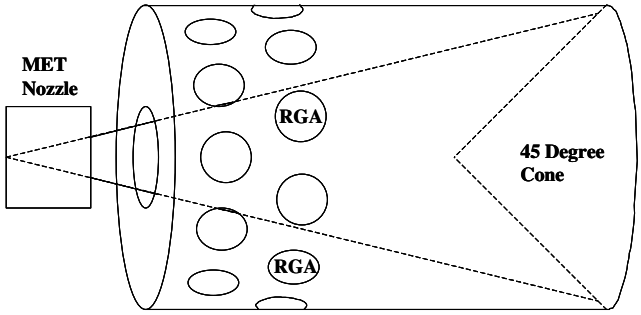

Fig. 6 Momentum trap. Effluent sampled at locations marked "RGA."

trap vent holes (Fig. 6). Outside the vacuum chamber the tubes were valved so that either one could be selected to supply gas to the residual gas analyzer (RGA). Sampling tubes were heated to between 65 and 95°C outside the vacuum chamber to improve response time for water, but the tubes inside the vacuum chamber were at room temperature. The pressure in the line to the RGA was probably close to the vacuum chamber pressure (∼13 Pa). Gas was admitted to the RGA through a leak valve and differentially pumped to approximately 3×10^{-4} Pa.

F. Operating Procedure

At flow rates of interest, the MET discharge chamber pressure was at least a significant fraction of atmospheric pressure. At such pressures it was not possible to form plasma without external intervention, such as insertion of a sharp electrode. A practical alternative was to achieve breakdown on the vacuum chamber background gas (air at a few Pa), then immediately introduce the desired propellant flow rate. For He, N_2, and N_2O, implementation of this procedure was trivial. Water was not as simple, because several minutes were typically required to establish a steady flow through the vaporizer. For the configuration lacking an isolator, the magnetron would not have been protected from the large amount of power reflected from the low pressure background discharge during this period. This problem was solved by placing a dummy orifice in parallel with the MET (Fig. 3). The orifice was sized to yield a vaporizer downstream pressure close to the expected MET discharge pressure. Steady flow was established through the dummy orifice, then switched to the MET. Additionally, before switching water flow to the MET, a helium discharge was established at a pressure comparable to that expected during water operation. This also minimized any abrupt change in pressure downstream of the vaporizer as flow was switched and avoided triggering vaporizer flow oscillations. Helium flow was gradually shut off within 10–20 s after the switch.

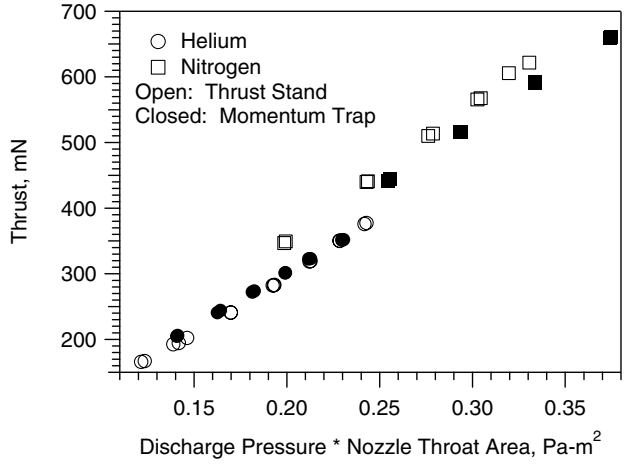

Fig. 7 Momentum trap validation.

For a given power level, the lower limit on the mass flow (upper limit on specific energy) was established by the point at which the plasma would expand to fill the entire discharge chamber. No data were taken in this condition, under the assumption that power loss to the chamber walls would be significantly enhanced relative to conditions for which a compact discharge was formed. Transition from a diffuse to a compact, oval shaped discharge adjacent to the nozzle inlet occurred abruptly as the mass flow rate was increased. This behavior has also been reported by Sullivan and Micci [16].

III. Results and Discussion

A. Data Reduction

The MET was evaluated through the experimental determination of thrust T, specific impulse I_{sp}, thrust efficiency η_T, and microwave coupling efficiency η_C. Specific impulse is defined as the ratio of thrust to propellant sea level weight flow:

$$I_{sp} = T/\dot{m}g \tag{1}$$

where g is the acceleration of gravity at sea level, and $\dot{m}$ is the propellant mass flow rate. Thrust efficiency for He, N_2, and N_2O was determined as the ratio of directed thrust power to total input power:

$$\eta_T = \frac{T_H^2}{2\dot{m}P_A + T_C^2} \tag{2}$$

where T_H is the "hot" thrust with microwave power, and T_C is the cold flow thrust. Inclusion of cold flow thrust accounts for propellant enthalpy entering the thruster. For water, the dominant contribution to propellant enthalpy entering the thruster came from vaporization. In this work no attempt was made to transfer waste heat from the thruster to incoming water, and water efficiency was calculated as

$$\eta_T = \frac{T_H^2}{2\dot{m}(P_A + P_V)} \tag{3}$$

where P_V is the power supplied to the vaporizer. P_A is the microwave power absorbed by the plasma:

$$P_A = P_I - P_{RM} - P_{RI} \tag{4}$$

where P_I is the input power to the magnetron, and P_{RM} and P_{RI} are the powers rejected in the magnetron and isolator cooling water supplies, respectively. Ohmic dissipation in the cavity walls was assumed to be negligible. Specific energy was calculated as $P_A/\dot{m}$.

For He, N_2, and N_2O the magnetron was bolted directly to the cavity, and P_{RM} was assumed to consist of waste heat from microwave generation as well as power reflected from the cavity. In this case we could not measure magnetron efficiency and decided to use the following definition for microwave coupling efficiency:

$$\eta_C = P_A/P_I \tag{5}$$

Coupling efficiency data presented in the next section suggest that over the investigated power range the efficiency of the 1 kW magnetron may have been approximately 73%.

The efficiency of the 5 kW magnetron, determined from measurements of P_{RM} in the configuration including an isolator, varied significantly over the investigated input power range (45–70% over 1–3 kW). Coupling efficiency with water uses the traditional definition:

$$\eta_C = P_A/(P_I\eta_M) \tag{6}$$

where η_M is the magnetron efficiency. In the interest of clarity, error bars are not present on any plots. Uncertainty in measured thrust for He, N_2, and N_2O was dominated by zero drift, resulting in an average absolute uncertainty of 2 mN (resolution 0.1 mN). Using standard techniques for the propagation of random measurement errors [18], we estimate the relative uncertainty in specific impulse to be 3%, and 5% for thrust and coupling efficiencies for those propellants. Thrust

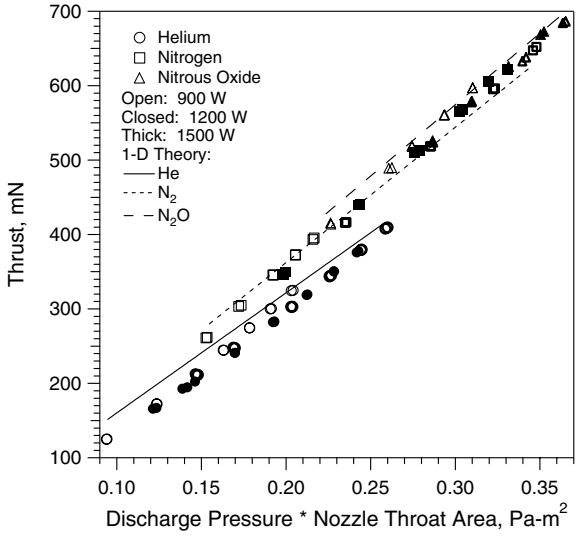

Fig. 8 Measured and calculated thrust for He, N_2, and N_2O.

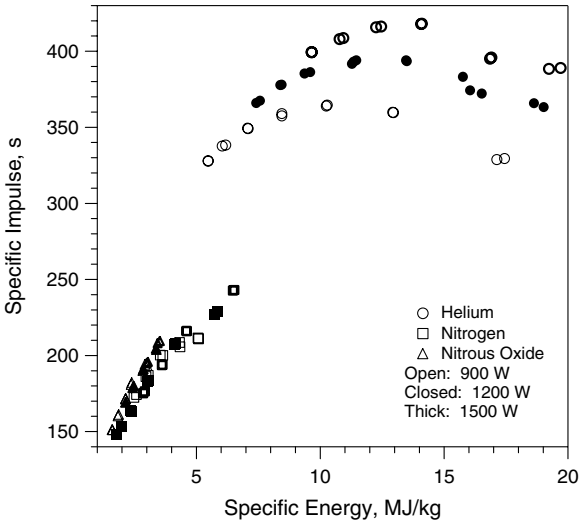

Fig. 9 He, N_2, and N_2O specific impulse.

uncertainty for water was estimated to be 5% based on the data of Fig. 7, however, it is not clear that those results are applicable to water or its decomposition products. Further characterization of the momentum trap is needed to answer this question. Under the assumption of a 5% uncertainty in thrust, we estimate the uncertainty in specific impulse and thrust efficiency to be 10%. The uncertainty in water coupling efficiency was estimated to be 5%. All relative uncertainties are percentages of the values plotted.

B. 1 kW MET

MET performance on He, N_2, and N_2O was measured at magnetron input powers of 900, 1200, and 1500 W with a nozzle throat diameter of 1.32 mm. Discharge pressure ranged from 6.7×10^4 to 1.9×10^5 Pa for He, 1.1×10^5 to 2.5×10^5 Pa for N_2, and 1.6×10^5 to 2.7×10^5 Pa for N_2O.

Figure 8 includes thrust calculated under the assumptions of one-dimensional, isentropic flow of a perfect gas with constant specific heats. Specific heat ratios of 5/3, 1.3, and 1.2 were used for He, N_2, and N_2O, respectively. The success of these calculations validates (for these propellants) the nearly universal practice in the MET literature of calculating performance based on measurements of discharge pressure and mass flow rate [2,3,5,6,8–10,12].

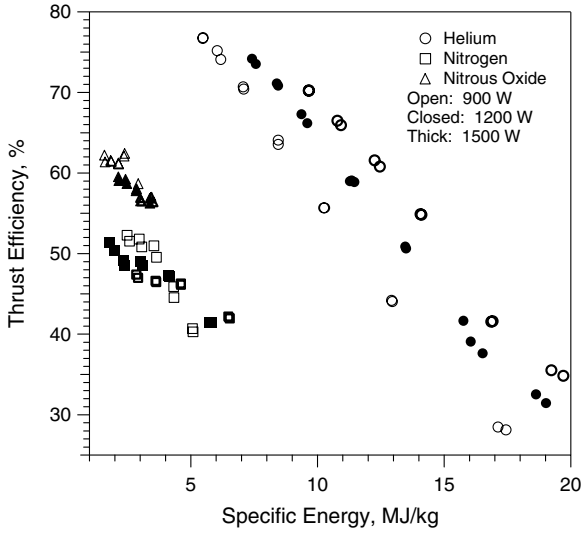

Fig. 10 He, N_2, and N_2O thrust efficiency.

Contrary to the behavior of conventional arcjets, Fig. 9 shows that the He specific impulse did not increase monotonically with specific energy. Plasma volume was observed to increase with increasing specific energy, presumably leading to increased power loss to the chamber walls, reduced thrust efficiency (Fig. 10), and the eventual decline of specific impulse. At a fixed value of specific energy, increasing power required corresponding increases in flow rate and pressure, resulting in higher thrust efficiency and specific impulse through the formation of more compact discharges. Although the rise of specific impulse with specific energy was monotonic for N_2 and N_2O, increasing specific energy beyond the peak values shown resulted in the sudden expansion of the plasma to fill the entire discharge chamber. As mentioned in Sec. II.F, no data were taken in this condition under the assumption that performance would be poor relative to operation with a compact discharge. Power frozen into dissociation of N_2 and N_2O presumably led to reduced thrust efficiency relative to He, and energy released from the decomposition of N_2O may have been responsible for higher efficiency relative to N_2.

Figure 11 shows that coupling efficiency increased with specific energy. It is noteworthy that values for all three propellants are similar, despite the fixed cavity geometry. The reader is reminded that with the 1 kW MET we had no means of measuring magnetron output (forward) power, and the definition of coupling efficiency used for the data of Fig. 11 [Eq. (5)] permits a maximum value equal to the magnetron efficiency.

C. 5 kW MET

The data of Fig. 10 were instructive for developing a strategy to run water with good efficiency. We first attempted to run water with the 1 kW MET and found that the available power was sufficient to sustain only diffuse discharges at relatively low pressure (less than 2.7×10^4 Pa), for which performance was poor. Our experience with other propellants indicated that increasing flow rate and pressure to achieve a compact water discharge would improve performance. Increased microwave power was required to sustain discharges at higher flow rates, hence the 5 kW magnetron.

Performance was recorded with compact water discharges at liquid flow rates from 1.8 to 4.5 cm^3/min (30 to 75 mg/s) and magnetron input powers from 2.1 to 4.1 kW. Discharge pressure varied from 4.0×10^4 to 1.5×10^5 Pa.

Figure 12 includes thrust calculated from an ideal expansion assuming a specific heat ratio of 1.2. The poor agreement with measured data indicates that the assumption of constant specific heats is not good for water, and that dissociation must be included to accurately predict performance. Figure 13 shows that specific impulse was nearly independent of specific energy over the

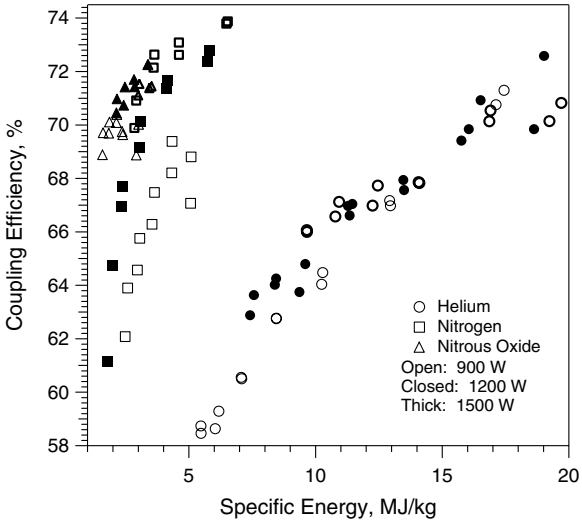

Fig. 11 He, N_2, and N_2O coupling efficiency [see Eq. (5)].

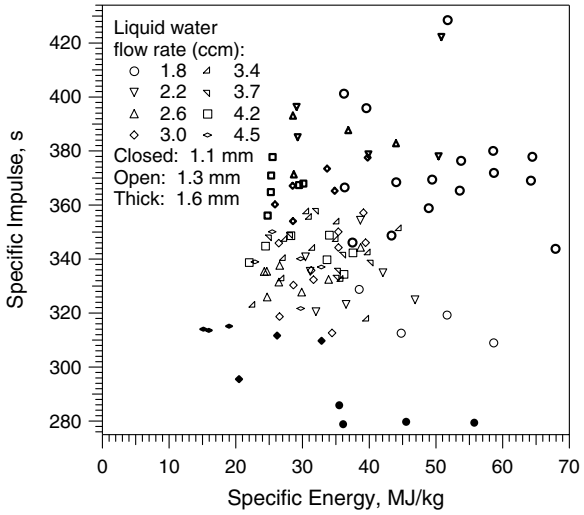

Fig. 13 Water specific impulse.

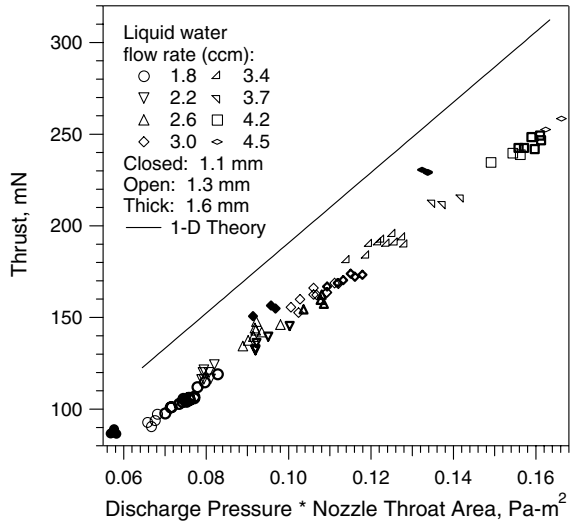

Fig. 12 Measured and calculated thrust for water.

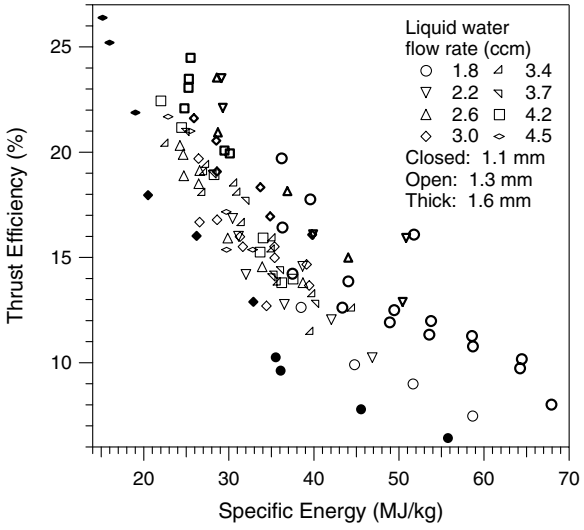

Fig. 14 Water thrust efficiency.

investigated range. A possible explanation for the lack of dependence on specific energy will be given in Sec. III.D. Increased nozzle throat area improved specific impulse, contrary to the prediction of idealized theory, which predicts that the largest nozzle expansion ratio should yield the largest thrust and specific impulse. We suspect that a smaller throat diameter enhanced power loss to the nozzle, though the mechanism has not been identified. Heat transfer through a boundary layer within the throat may have been responsible, or buoyancy may have forced the plasma into contact with the nozzle inlet cone. The force of buoyancy on the plasma might be larger for a given flow rate and temperature with a smaller throat due to the larger average density in the discharge chamber. The two exceptional data points at a specific energy of approximately 50 MJ/kg with the 1.57 mm nozzle (specific impulse above 420 s) may have resulted from fortuitous positioning of the plasma relative to the nozzle inlet.

Enhanced power loss with reduced nozzle throat size is also evident in the thrust efficiency data of Fig. 14. As with the other propellants, efficiency decreased with increasing specific energy due to increased plasma volume and consequent increased power loss to the chamber walls. Low efficiencies relative to the other propellants were possibly due to a combination of power frozen into dissociation, enhanced heat transfer to the cavity walls due to the high thermal conductivity of hydrogen, and the use of a separate power source for water vaporization.

Figure 15 shows that microwave coupling efficiencies for water were high, further demonstrating the versatility of the fixed geometry MET. As with the other propellants, coupling efficiency improved with increasing specific energy.

Figure 16 shows microwave coupling efficiency recorded with water in the tunable configuration with a 1.32 mm nozzle and with stubs adjusted for minimum reflected power. Operation covered magnetron input powers from 2 to 3 kW, discharge pressures from 4.4×10^4 to 1.4×10^5 Pa, and thrust from 78 to 293 mN. Coupling efficiencies greater than 96% were achieved over a broad range of specific energy, but did not result in increased specific impulse (Fig. 17). A few measurements of specific impulse were actually lower than those presented in Fig. 13 for the same nozzle, though the difference is within measurement uncertainty.

D. Water Dissociation

As described in Sec. II.E, effluent from the momentum trap during operation with water was sampled with a residual gas analyzer. After mixing in the water-cooled momentum trap, and traveling through sections of room temperature tubing, only the stable molecular species H_2O, H_2, and O_2 arrived at the RGA. After background subtraction and scaling for the RGA sensitivity to each species, we obtained data indicating that the amount of H_2 was nearly equal to or less than the amount of O_2. This is a nonphysical result, because the

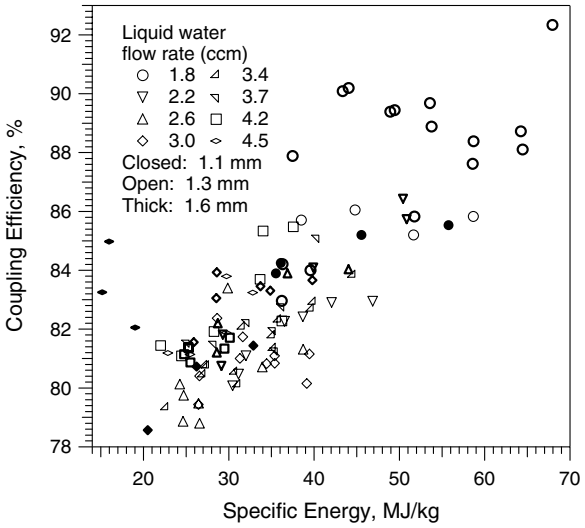

Fig. 15 Water coupling efficiency [see Eq. (6)].

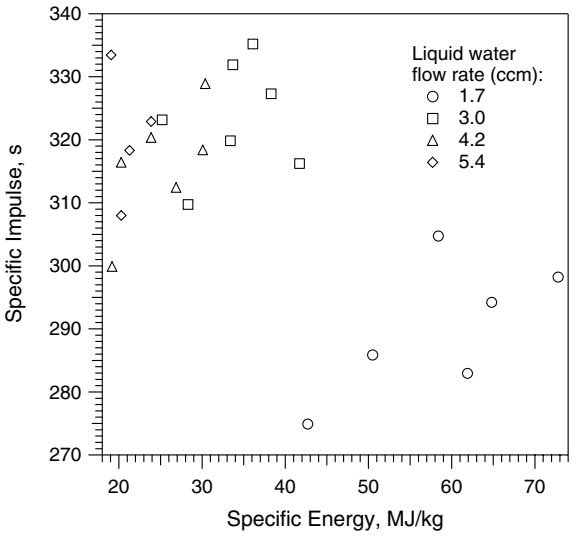

Fig. 17 Water specific impulse with tuning.

amount of H_2 must be twice that of O_2. A possible explanation is that the lighter H_2 expanded rapidly as it exited the thruster and was preferentially excluded from the momentum trap entrance aperture. Figure 18 shows the results for operation at flow rates of 1.8, 3.0, and 4.2 cm^3/min at magnetron input powers from 2 to 2.5 kW, under the assumption that the amount of H_2 was equal to twice the measured amount of O_2. Data from both sampling tubes are presented, but no distinction between tubes is made because results obtained from each were very similar.

Figure 18 indicates that the water plume was at least 30– 40% dissociated. The actual value was almost certainly higher because the amount of H, O, and OH in the plume that was converted to H_2O in the momentum trap or the lines to the RGA was unknown. A chemical kinetics program called CHEMKIN [19] employing the reaction set specified in GRI-Mech 3.0 [20] was used to estimate the true level of dissociation. Our procedure was to postulate a discharge chamber composition by solving for the equilibrium composition of H_2O at an assumed temperature and at a pressure near measured values. This composition was assumed to persist through the nozzle expansion and was input to CHEMKIN as reactants at 13 Pa and 300 K, roughly the conditions pertaining to the momentum trap and sampling tubes. CHEMKIN solved for species present after 1 min, approximately the time required to reach steady state readings at the RGA.

Table 1 lists equilibrium compositions for water at 0.5 atm (approximate discharge pressure at 1.8 cm^3/min) and 3100 K, and at 1 atm (approximate discharge pressure for 3.0 and 4.2 cm^3/min) and 3500 K. After 1 min at 13 Pa and 300 K, the compositions shown in Table 2 were obtained, closely matching the data of Fig. 18 (specific energies above 40 MJ/kg correspond to 1.8 cm^3/min). It appears possible that the actual level of water dissociation in the plume was 50–70%.

A few calculations can be made using the temperature and composition data in Table 1, the results of which are shown in Table 3. Ideal I_{sp} for each mixture was calculated from the mass averaged velocity. Species velocities were determined by assuming complete conversion of sensible enthalpy to directed kinetic energy. Enthalpies were obtained from tabulated values [21] for all species except atomic hydrogen. The enthalpy of atomic hydrogen was set to $5/2RT$, where R is the specific gas constant for H and T is the temperature in K. Values of ideal I_{sp} compare favorably with our measured values.

The fourth column of Table 3 lists the sensible enthalpy of each mixture per kg of H_2O. The last column lists the enthalpy invested in dissociation. With this information we can estimate the relative importance of dissociation as an energy sink. In the 1 atm case, the sum of the sensible enthalpy and enthalpy of dissociation is about 24 MJ/kg, which is comparable to input specific energies for this

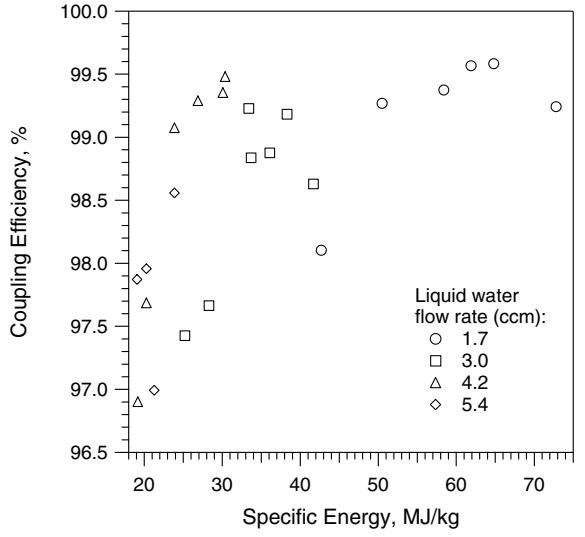

Fig. 16 Water coupling efficiency with tuning.

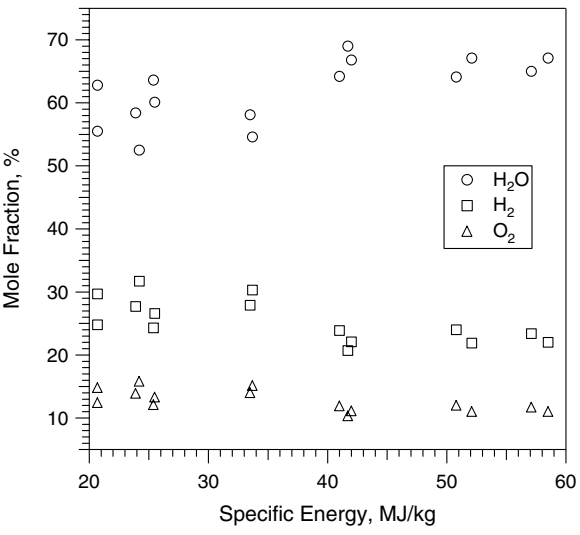

Fig. 18 Species resent at RGA.

Table 1 Prospective plume compositions

Atm	K	H_2O	H	H_2	OH	O	O_2
0.5	3100	47%	12%	17%	12%	6%	6%
1.0	3500	30%	20%	20%	15%	10%	5%

Table 2 Prospective detectable species

Table 1	H_2O	H_2	O_2
0.5 atm	67%	22%	11%
1.0 atm	58%	28%	14%

Table 3 Results of calculations using data from Table 1

Atm	K	Ideal I_{sp}, s	Sensible enthalpy, MJ/kg_{H_2O}	Enthalpy of dissociation, MJ/kg_{H_2O}
0.5	3100	395	8.3	8.6
1.0	3500	410	9.8	13.8

operating pressure (20 to 35 MJ/kg). In this case dissociation is the dominant energy sink, consuming roughly half of the power absorbed in the plasma. At 0.5 atm, input specific energies range from about 35 to 70 MJ/kg, so that sensible enthalpy and enthalpy of dissociation each account for 12–25% of the power absorbed by the plasma, indicating that another energy sink must be present to absorb the remaining 50–75%. We suspect this sink is heat transfer to the walls of the discharge chamber, because plasma volume increases with increasing specific energy, resulting in increased surface area for radiation and closer proximity for convection and conduction to the walls. Power inputs to the discharge chamber structure were crudely estimated from thermocouple data by assuming that each component was uniformly at the measured temperature and that no heat was lost to conduction or radiation. Dividing by the relevant water flow rate yielded a heat transfer specific energy of 28 MJ/kg at high input specific energy (60 to 70 MJ/kg), indicating that heat transfer was about 3 times as important as dissociation. At low input specific energy (20 to 30 MJ/kg), the result was 6 MJ/kg, less than half as important as dissociation.

This crude experiment has suggested an explanation for why water specific impulse was nearly independent of specific energy. At low specific energy the plasma was compact with low power loss to the thruster body but large loss to dissociation. The relative importance of dissociation was reduced by increasing the input specific energy, but this led to expansion of the plasma and increased heat transfer to the thruster body. The net result was a nearly constant value of sensible enthalpy available for conversion to directed kinetic energy.

IV. Conclusion

Thrust, specific impulse, thrust efficiency, and microwave coupling efficiency were measured for a nominally 1 kW MET operating on He, N_2, and N_2O, and for a nominally 5 kW MET operating on water. For He, N_2, and N_2O, measured thrust agreed well with idealized calculations. Specific impulse for He displayed a maximum when plotted against specific energy, possibly because of enhanced power loss to the discharge chamber walls as increasing specific energy led to increased plasma volume. Wall losses were apparently also responsible for the decline of thrust efficiency with increasing specific energy for all four propellants. Because of the influence of dissociation, agreement with idealized calculation was worse for water thrust, and water thrust efficiency was well below that of the other propellants. Specific impulse for water was nearly independent of specific energy. Despite the lack of an impedance matching capability in the compact MET design, coupling efficiencies were high for all propellants, and increased with increasing specific energy. The addition of impedance matching increased microwave coupling efficiencies to greater than 96% for water, but did not improve specific impulse. A crude arrangement with a residual gas analyzer revealed that the water plume may be 50–70% dissociated, and that dissociation is the dominant power sink at low specific energy whereas heat loss to the thruster body dominates at high specific energy.

Acknowledgments

This work was supported under The Aerospace Corporation's Independent Research and Development program. The MET resonant cavity was provided by Research Support Instruments. The authors gratefully acknowledge many useful discussions with Dan Sullivan regarding design of the impedance matching system.

References

[1] Asmussen, J., Mallavarpu, R., Hamann, J. R., and Park, H. C., "The Design of a Microwave Plasma Cavity," *Proceedings of the IEEE*, Vol. 62, No. 1, Jan. 1974, pp. 109–117.

[2] Whitehair, S., Asmussen, J., and Nakanishi, S., "Microwave Electrothermal Thruster Performance in Helium Gas," *Journal of Propulsion and Power*, Vol. 3, No. 2, March–April 1987, pp. 136–144.

[3] Herlan, W. A., and Jassowski, D. M., "Microwave Thruster Development," AIAA Paper 87-2123, June 1987.

[4] Tahara, H., Abuku, M., Yasui, T., Onoe, K., and Yoshikawa, T., "Performance Characteristics of Plasmajets and Ion Sources Using Resonant-Cavity Microwave Discharge," AIAA Paper 90-2633, July 1990.

[5] Balaam, P., and Micci, M. M., "Performance Measurements of a Resonant Cavity Electrothermal Thruster," IEPC Paper 91-031, 1991.

[6] Sullivan, D. J., and Micci, M. M., "The Effect of Molecular Propellants on the Performance of a Resonant Cavity Electrothermal Thruster," IEPC Paper 91-034, 1991.

[7] Power, J. L., "Microwave Electrothermal Propulsion for Space," *IEEE Transactions on Microwave Theory and Techniques*, Vol. 40, No. 6, June 1992, pp. 1179–1191.

[8] Balaam, P., and Micci, M. M., "Investigation of Stabilized Resonant Cavity Microwave Plasmas for Propulsion," *Journal of Propulsion and Power*, Vol. 11, No. 5, Sept.–Oct. 1995, pp. 1021–1027.

[9] Richardson, W., and Asmussen, J., "Coaxial Microwave Electrothermal Thruster Performance in Hydrogen," NASA CR-196839, 1994.

[10] Sullivan, D. J., Kline, J., Philippe, C., and Micci, M. M., "Current Status of the Microwave Arcjet Thruster," AIAA Paper 95-3065, July 1995.

[11] Brandenburg, J. E., and Micci, M. M., "The Microwave Electro-Thermal (MET) Thruster: A New Technology for Satellite Propulsion and Attitude Control," *AIAA/Utah State University 9th Annual Conference on Small Satellites*, Utah State University, Logan, UT, 1995.

[12] Sullivan, D. J., and Micci, M. M., "Development of a Microwave Resonant Cavity Electrothermal Thruster Prototype," IEPC 93-036, Sept. 1993.

[13] Mallavarpu, R., Asmussen, J., and Hawley, M. C., "Behavior of a Microwave Cavity Discharge Over a Wide Range of Pressures and Flow Rates," *IEEE Transactions on Plasma Science*, Vol. PS-6, No. 4, Dec. 1978, pp. 341–354.

[14] Frasch, L. L., Griffin, J. M., and Asmussen, J., "An Analysis of Electromagnetic Coupling and Eigenfrequencies for Microwave Electrothermal Thruster Discharges," AIAA Paper 87-1012, May 1987.

[15] Morren, W. E., "Gravity Sensitivity of a Resistojet Water Vaporizer," AIAA Paper 93-2402, June 1993.

[16] Sullivan, D. J., and Micci, M. M., "Performance Testing and Exhaust Plume Characterization of the Microwave Arcjet Thruster," AIAA Paper 94-3127, June 1994.

[17] Cheng, D. Y., and Chang, C. N., "Deflagration Plasma Thruster," *Orbit-Raising and Maneuvering Propulsion: Research Status and Needs*, AIAA, New York, 1984, pp. 371–384.

[18] Bevington, P. R., *Data Reduction and Error Analysis for the Physical Sciences*, McGraw–Hill, New York, 1969.

[19] Kee, R. J., Rupley, F. M., Miller, J. A., Coltrin, M. E., Grcar, J. F., Meeks, E., Moffat, H. K., Lutz, A. E., Dixon-Lewis, G., Smooke, M. D., Warnatz, J., Evans, G. H., Larson, R. S., Mitchell, R. E., Petzold, L. R., Reynolds, W. C., Caracotsios, M., Stewart, W. E., Glarborg, P., Wang, C., Adigun, O., Houf, W. G., Chou, C. P., and Miller, S. F., Chemkin Collection, Release 3.7, Reaction Design, Inc., San Diego, CA, 2002.

[20] Smith, G. P., Golden, D. M., Frenklach, M., Moriarty, N. W., Eiteneer, B., Goldenberg, M., Bowman, C. T., Hanson, R. K., Song, S., Gardiner, W.C., Lissianski, V. V., and Qin, Z., "GRI-Mech 3.0," http://www.me.berkeley.edu/gri_mech/ [cited 2006].

[21] Wark, K., *Thermodynamics*, 4th ed., McGraw–Hill, New York, 1983.

R. Myers
Associate Editor